Origin of glass forming ability of Cu-Zr alloys: A link between compositional variation and stability of liquid and glass

Shraddha Ganorkar,[1] Sooheyong Lee,[1,2] Yun-Hee Lee,[1,2] Takehiko Ishikawa,[3] and Geun Woo Lee[1,2,*]
[1]*Division of Industrial Metrology, Korea Research Institute of Standards and Science, 305–340, Republic of Korea*
[2]*Department of Nano Science, University of Science and Technology (UST), Daejeon 305–350, Republic of Korea*
[3]*Japan Aerospace Exploration Agency, Tsukuba Space Center, 2-1-1 Sengen, Tsukuba, Ibaraki 305–8505, Japan*

(Received 26 February 2018; revised manuscript received 4 October 2018; published 29 November 2018)

Here, we provide a link which shows how the compositional change affects the liquid and glass stabilities by measuring temperature-time transformation (TTT) diagram of Cu-Zr alloys, revealing the origin of glass forming ability (GFA) with composition. From the TTT study, we find that the compositional change yields a different origin of GFA for the three best bulk metallic glasses ($Cu_{64}Zr_{36}$, $Cu_{56}Zr_{44}$, and $Cu_{50}Zr_{50}$) due to varying stabilities of liquid and glass, which explains maxima observed in undercoolability, persisting time at nose temperature, and crystal-liquid interfacial free energy.

DOI: 10.1103/PhysRevMaterials.2.115606

Evaluation of glass forming ability (GFA) is indispensable for the fundamental understanding of bulk metallic glass (BMG) formation by small additions or compositional change, as well as for materials processing (e.g., designing, casting, and annealing) and prediction of BMGs [1–4]. GFA is gauged by the degree of supercooling of liquid (i.e., liquid stability) and resistance of the glassy phase against crystallization (i.e., glass stability). Presently, many GFA parameters have been proposed based on the liquid stability and glass stability [5–7], but often failed to predict the GFA in many BMGs [7–9], which still forces one to find new criterion [10].

Cu-Zr alloys have been candidates and intensively studied to reveal the origin of GFA, due to its compositional simplicity, largely different GFA with minute compositional change [11], and as a base material for many multicomponent BMGs. However, the proposed GFA parameters [12,13] failed to predict the formation of Cu-Zr BMGs. Moreover, at a certain composition, it exhibits various peculiar anomalies in density [11] or atomic packing density [14,15], thermal expansion [16], enthalpy difference between amorphous and crystal [17,18], and undercoolability and interfacial free energy [19,20]. The origin of the failure and the anomalies has not been revealed yet, and correlation of the compositional change and the stability of liquid and glass for the GFA is still ambiguous.

The relation of small compositional change and the stability of liquid and glass can be understood by structural viewpoint. Icosahedral short-range order (ISRO), widely recognized to underlie the stability of supercooled liquid [21], has been supported by experimental [22–26] and simulation [27–29] studies, also known to enhance crystal-liquid interfacial free energy, and thus suppressing crystallization [30]. However, a geometric model for the density anomaly [31] and continuously decreasing population of a fivefold cluster with increasing Zr concentration [32,33] (i.e., deteriorating liquid stability) could not explain the GFA of Cu-Zr BMGs with composition. As alternative causes affecting GFA, simulation studies [31–35] suggested the imperfect ISRO, other polyhedra, or the formation of ISRO networks for dense atomic packing and slowing down dynamics which enhanced glass stability.

Although those simulation studies may infer the essence of GFA with the compositional change and the liquid and glass stabilities in Cu-Zr alloys, experimental vindication has not yet happened. Evidence of the stability change in liquid and glass with composition can be provided by the temperature-time transformation (TTT) diagram, since the C shape of the TTT curve is formed by two characteristic times for the supercooled liquid [i.e., τ_n for crystallization (thermodynamics) and τ_d for diffusion or relaxation (kinetics), reflecting the two stabilities] as shown in Fig. 1. The upper half of the C curve indicates stability of supercooled liquid due to the dominated nucleation, while the lower half is related to stability of glass due to the dominated relaxation behavior of the supercooled liquid [36]. If compositional change enhances the liquid stability, τ_n will increase, resulting in lowering nose temperature T_n (the temperature taking the shortest time for crystallization) and rising nose time (t_n) [Fig. 1(b)]. On the other hand, if glass stability (i.e., relaxation or viscosity) is reinforced, τ_d will increase, yielding higher T_n, and longer t_n for crystallization [Fig. 1(c)]. If both stabilities of liquid and glass become equivalently better with compositional change, the TTT curve moves toward longer time without changing T_n [Fig. 1(d)].

Accordingly, if the compositional change results in structural modification affecting liquid or glass stability and finally yielding the anomalies as the signatures of good GFA, the respective impacts of compositional change should appear in the TTT curve. Presently, however, only a few theoretical and simulation TTT studies of Cu-Zr alloys [36–38] have been performed, showing contradictory behaviors due to unavailable thermophysical properties of supercooled liquids.

*Corresponding author: gwlee@kriss.re.kr

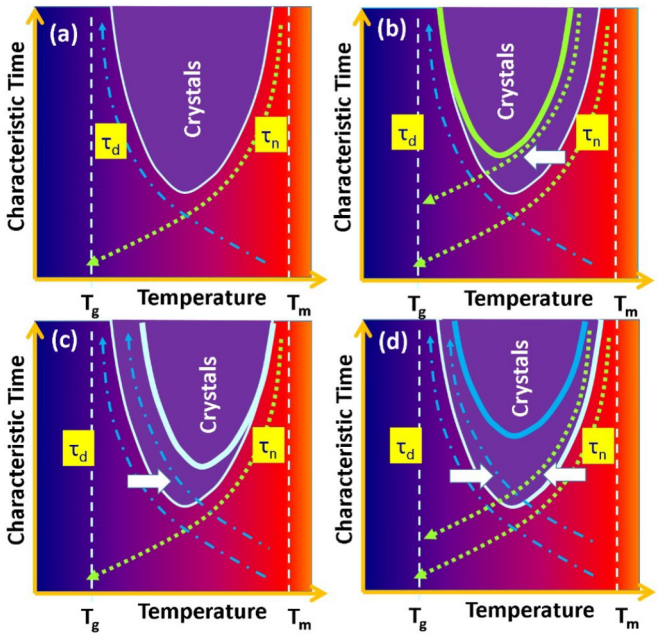

FIG. 1. Schematic features of TTT curves reflecting the change of liquid and glass stabilities. (a) shows the C curve formed by the two characteristic times for nucleation (τ_n) and diffusion (τ_d). (b) shows longer nose time (t_n) and lower nose temperature (T_n) due to increasing τ_n (i.e., increasing liquid stability). (c) is of longer t_n and higher T_n due to increasing τ_d (i.e., increasing glass stability). (d) shows the enhanced stabilities in liquid and glass sides due to increasing both characteristic times.

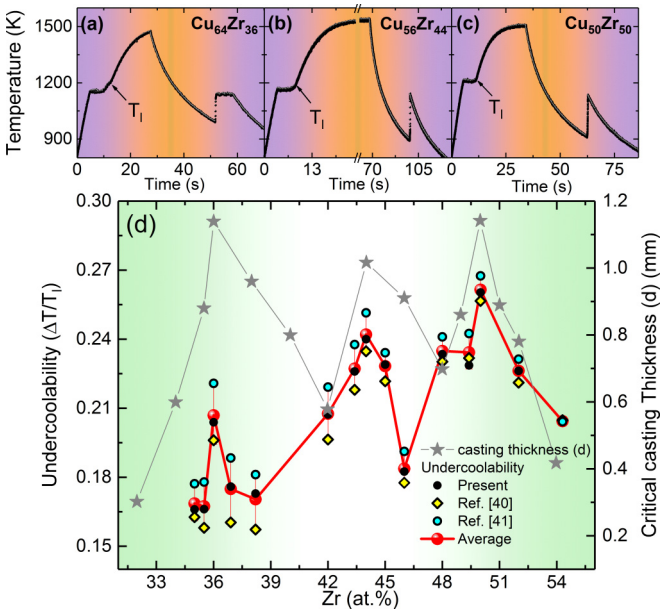

FIG. 2. Temperature-time curves for $Cu_{64}Zr_{36}$, $Cu_{56}Zr_{44}$ and $Cu_{50}Zr_{50}$ alloys, where arrows show the liquidus temperatures (a)–(c). Undercoolability as a function of Zr concentration is plotted with critical casting thickness, extracted from Ref. [11] (d). The undercoolability data are deduced by three different T_l from the present study, Refs. [40] and [41]. The averaged undercoolability from the three liquidus temperature is shown with red dots and red line.

In this work, we provide experimental demonstration by measuring the TTT curve wherein the compositional change produces different influence on the stability of liquid and glass, indicating a different origin of GFA for the best Cu-Zr BMGs. This has been strongly suspected, but never clarified. More, maxima in the crystal-liquid interfacial free energy imply that the compositional change causes a large structural difference of liquid and crystal in SRO and MRO (medium range order), and thus ultimately results in different stability of liquid and glass for the best Cu-Zr BMGs. The present results provide profound insight and strong impact to improve the GFA of BMGs by adding elements and changing compositions.

The stability of supercooled liquid is studied by undercooling experiments. Figures 2(a)–2(c) show typical time-temperature curves of $Cu_{64}Zr_{36}$, $Cu_{56}Zr_{44}$ and $Cu_{50}Zr_{50}$ alloys in the electrostatic levitation (ESL) technique (Fig. S1 in the Supplemental Material [39]). In Fig. 2(d), the undercoolability ($\Delta T/T_l = (T_l - T_r)/T_l$, where T_l is a liquidus temperature, and T_r is a recalescence temperature) is obtained with three different T_l from the present experiment, and two reported phase diagrams [40,41].

Interestingly, the undercoolability exhibits three maxima, 0.206 ± 0.012, 0.242 ± 0.008, 0.261 ± 0.005 at $Cu_{64}Zr_{36}$, $Cu_{56}Zr_{44}$, and $Cu_{50}Zr_{50}$, respectively [Fig. 2(d)], which is consistent with the maxima of critical casting thickness of Cu-Zr BMGs [11], and other maxima [16,18,20]. The higher undercoolability of the three compositions indicates better liquid stability than their neighbors, implying a higher nucleation barrier for crystallization.

Figure 3 shows the TTT curves of the selected Cu-Zr alloy liquids with fitting curves using the classical nucleation theory (CNT) [42]. All thermophysical properties were measured for this fitting (See Fig. S1–S4 and Table S1 in the Supplemental Material [39]).

In each BMG group, the calculated TTT curves of $Cu_{64}Zr_{36}$, $Cu_{56}Zr_{44}$, and $Cu_{50}Zr_{50}$ show longer persistence times (t_n) than their neighbors at T_n, which are of $\sim 1.37 \times 10^{-3}$ s, $\sim 6 \times 10^{-1}$ s, ~ 1.25 s, for three BMGs, respectively. These results are consistent with undercoolability in Fig. 2(d) and other anomalies found in the previous studies [11,16,18,20]. Interestingly, the nose temperature of the $Cu_{50}Zr_{50}$ liquid is higher than its neighbors, unlike $Cu_{64}Zr_{36}$, and $Cu_{56}Zr_{44}$. This causes the shorter persistence time of $Cu_{50}Zr_{50}$ liquid as compared to its neighbors above a supercooled temperature 890 K, which is counterintuitive from the undercoolability.

For comparing these results at an equivalent condition, the TTT curves are normalized by T_l and T_g (glass transition temperature), since the alloys have different T_l and T_g. The normalized TTT curves will expose whether nucleation or viscosity affects the GFA dominantly. The normalized TTT curves by T_l are given in Figs. 4(a)–4(c). Above normalized T_n where thermodynamics (i.e., nucleation) is dominated, $Cu_{64}Zr_{36}$ exhibits longer persistence time (Δ_t and t_n) in the supercooled state, compared to their neighboring compositions [Figs. 4(a) and 4(d)].

Based on CNT [42], the nucleation barrier (ΔG^*) resisting the crystallization is given by $\Delta G^* \sim \sigma^3/(\Delta G_v)^2$, where σ is the crystal-liquid interfacial free energy and ΔG_v

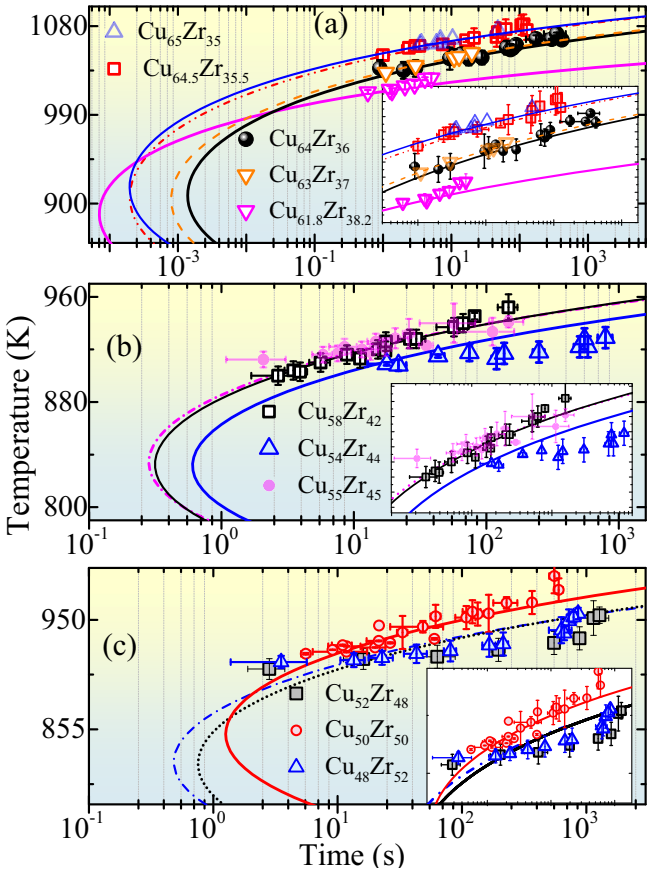

FIG. 3. TTT diagram of $Cu_{100-x}Zr_x$ alloys for $x = 35$, 35.5, 36, 37, and 38 (a), for $x = 42$, 44, and 45 (b), for $x = 48$, 50, and 52 (c). Fitting lines by CNT are shown through the experimental data. The overlapping of TTT curves indicates the similarity in undercoolability of the compositions before and after local maxima (Fig. 2).

is the volume Gibbs free energy difference between liquid and crystal. Here, identical reduced temperature implies an equivalent driving force for the nucleation, if we assume that fusion enthalpies are almost the same within each group due to their small compositional change (for instance, in case of Turnbull's approximation, $\Delta G_v = \Delta H_f(1 - T/T_l)$, where ΔH_f is the fusion enthalpy). Thus, the nucleation is mainly governed by σ. In short, the longer persistence time of the supercooled liquid reflects a better liquid stability due to a higher σ in the $Cu_{64}Zr_{36}$ group. In the case of $Cu_{56}Zr_{44}$, and $Cu_{50}Zr_{50}$, t_n is longer than their neighbors, indicating better GFA. However, their persistence time of supercooled liquid (Δt_n) does not systematically vary with Zr concentration, as shown in the $Cu_{64}Zr_{36}$ group. In addition, $Cu_{56}Zr_{44}$ and $Cu_{50}Zr_{50}$ show higher T_n than their neighbors. The above result implies that the origin of GFA differs from the $Cu_{64}Zr_{36}$ to $Cu_{56}Zr_{44}$ and $Cu_{50}Zr_{50}$ groups with changing Zr concentration.

To evaluate glass stability, TTT curves are normalized by T_g in Figs. 5(a)–5(c). Below T_n where the viscosity effect is dominant, Δt_n of all supercooled $Cu_{64}Zr_{36}$, $Cu_{56}Zr_{44}$ and $Cu_{50}Zr_{50}$ liquids are longer than their neighbors indicating better glass stability. Interestingly, $Cu_{50}Zr_{50}$ shows distinctly higher T_n than its neighbors [Fig. 5(c)].

According to the normalized TTT curves in Figs. 4 and 5, the change of Zr concentration produces better stability on both liquid and glass sides for $Cu_{64}Zr_{36}$ than its neighbors, which corresponds to the case of Fig. 1(d). In the case of $Cu_{56}Zr_{44}$, glass stability becomes better than its neighbors, whereas its liquid stability is not always better [e.g., $T/T_l = 0.8$ in Fig. 4(e)]. For the last group, the compositional change significantly enhances the glass stability of $Cu_{50}Zr_{50}$ as compared to its neighbors, which belongs to the case of Fig. 1(c). These surprising results indicate that the small change of Zr concentration has a different impact on liquid and glass stabilities in each group, yielding the different origin of GFA in the Cu-Zr BMGs. It is worth emphasizing that $Cu_{50}Zr_{50}$ shows better stability of liquid and glass than the other two best BMGs, as shown in Figs. 5(d) and 5(e).

Critical cooling rate R_c calculated from by $R_c = (T_l - T_n)/t_n$ are found to be 1.97×10^5, 545 and 289 K/s for $Cu_{64}Zr_{36}$, $Cu_{56}Zr_{44}$ and $Cu_{50}Zr_{50}$, respectively (See Table S1 for R_c in the Supplemental Material [39]), which significantly differ from the theoretical values [36,37,43–45] by a few orders of magnitude. In the case of $Cu_{50}Zr_{50}$, the present result, R_c (289 K/s) is found quite close to ~250 K/s, which was experimentally estimated by the critical casting diameter method [45].

We now discuss how compositional change differently influences the GFA of Cu-Zr BMGs. That is, how does the evolution of local orders with Zr concentration affect thermodynamics (i.e., nucleation) and kinetics (i.e., viscosity) in Cu-Zr liquids? The variation of Zr concentration should accompany a change of the local orders in liquids. It has been believed that ISRO as the local order plays a key role in stabilizing the liquids and glasses. On the other hand, structural heterogeneity caused by the networked or extended ISRO or icosahedral medium range order (IMRO) can increase viscosity affecting the glass stability. In Cu-Zr alloys, the two aspects have been scrutinized by simulation studies [32,33,46], the population; $Cu_{64}Zr_{36}$ has the larger number of ISRO than $Cu_{50}Zr_{50}$, lowering system energy and thus giving better liquid stability, and $Cu_{50}Zr_{50}$ has the larger number of IMRO than $Cu_{64}Zr_{36}$, slowing down kinetics and thus yielding better glass stability. This is consistent with the present TTT study in Figs. 4 and 5. Although the scenario explains the overall aspect for the formation of BMGs with Zr concentration, the monotonically decreasing number of ISRO and increasing number of the IMRO with Zr concentration in the liquids cannot simply account for the formation of the three best Cu-Zr BMGs at the specific compositions.

Another possible effect of the local structure change by Zr concentration is the crystal-liquid interfacial free energy (σ) which results from the configurational entropy difference (i.e., local structure difference) between liquid and crystal [47]. We estimate σ of Cu-Zr alloys as a function of Zr concentration (Fig. 6), which were obtained in two different ways, i.e., maximum undercooling and TTT curves, using CNT (see the details of the calculations in the Supplemental Material [39]). The estimated σ with Zr concentration shows three maxima at the three best BMG compositions, which is consistent with other maxima reported previously [11,16,18,20].

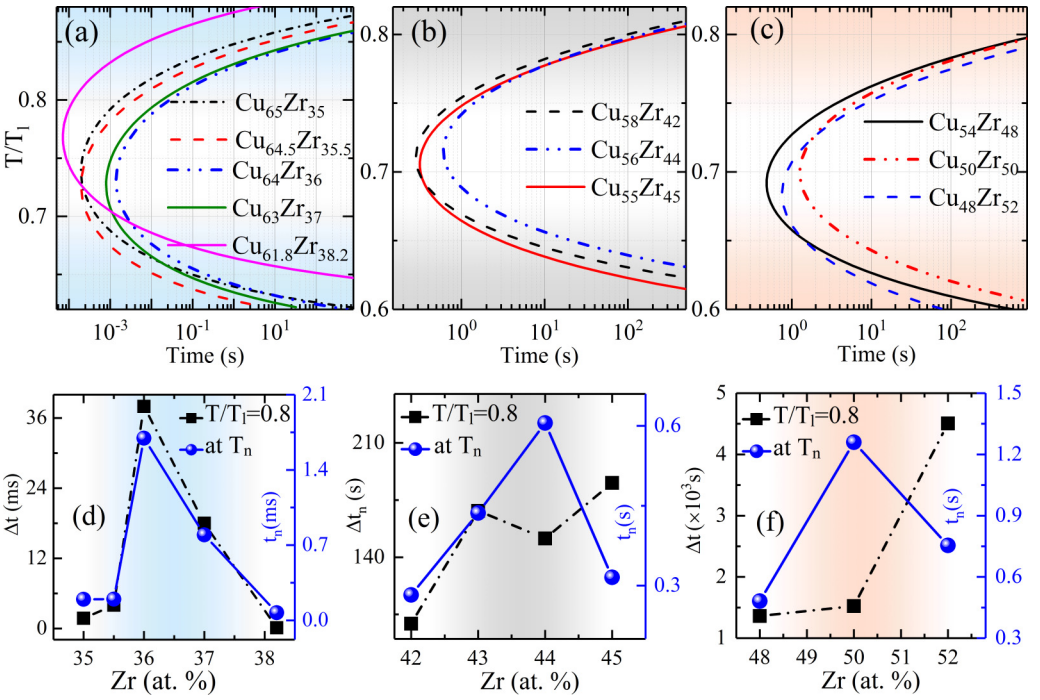

FIG. 4. TTT curves of Cu-Zr alloys normalized with T_l [(a)–(c)] and persistence time t_n at T_n and Δ_t at $T/T_l = 0.8$ [(d)–(f)].

The anomaly in σ reflects that the local ordering sensitively changes with Zr concentration, resulting in maximizing liquid stability as well as glass stability at the best BMG compositions. According to the simulation studies [32,33,35], the population of ISRO is large in the $Cu_{64}Zr_{36}$ group, while the number of ISRO networks (i.e., IMRO or extended ISRO) is dominated in the $Cu_{50}Zr_{50}$ group. Thus, the anomaly in the σ in Fig. 6 may be primarily attributed to the SRO for the $Cu_{64}Zr_{36}$ group, and the medium range order (MRO) for $Cu_{50}Zr_{50}$ group, respectively.

The above findings raise an interesting question. If glass stability is significantly dominant as MRO further evolves

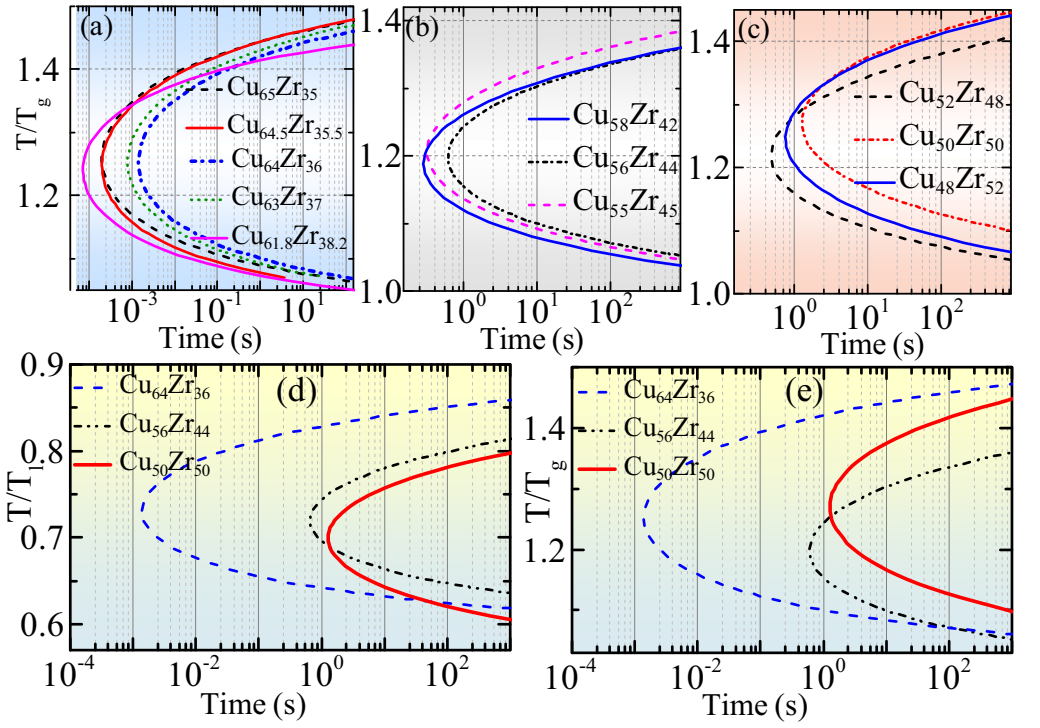

FIG. 5. TTT curves of Cu-Zr alloys normalized by T_g [(a)–(c)]. TTT curves of the three best BMG compositions normalized with T_l (d) and T_g (e).

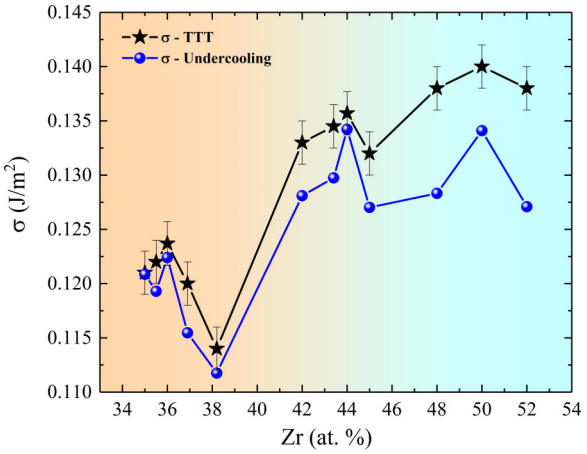

FIG. 6. The crystal-liquid interfacial free energy of Cu-Zr alloys as a function of Zr concentration which is estimated from maximum undercooling (circles) and TTT curves (stars). The three best BMGs show maximum values of crystal-liquid interfacial free energy.

by adding more elements (i.e., multicomponent liquids with high viscosity), how should the liquid stability appear? In this case, the nose temperature of the TTT curve moves significantly closer to the liquidus temperature with increasing nose time as shown in Fig. 1(c). This is because of the strong contribution of τ_d (i.e., strong glass stability). That is, τ (time for crystallization) $\sim\tau_d \gg \tau_n$. As a result, the liquid stability governed by thermodynamics (i.e., nucleation) is also strongly influenced by kinetics (i.e., viscosity), since the nucleation is also dependent on viscosity. Thus, in the case of highly viscous BMGs, the liquid stability did not explicitly appear in a previous study [48], although we expect deep supercooling and have the BMGs. Recently, Johnson *et al.* suggested that the GFA of BMGs can be explained by only two factors, i.e., Turnbull's parameter T_{rg} and Angel's fragility parameter m, but not the σ explicitly [49]. They explained that the σ might be implicitly included in those two parameters that could dominate incubation time for crystal nuclei formation by local chemical fluctuation in multicomponent liquids particularly. In short, like $Cu_{50}Zr_{50}$, better glass stability with higher interfacial free energy, causing higher undercoolability, may be a *precursor* that glass stability interferes in liquid stability.

In summary, we have demonstrated an essential link between compositional change and stability of supercooled liquid and glass (i.e., thermodynamics and kinetics). From the TTT study, we found that the change of Zr concentration reinforced both stabilities of the supercooled liquid and glass for $Cu_{64}Zr_{36}$, while it distinctly enhanced the glass stability for $Cu_{50}Zr_{50}$, by comparison with their neighbors. The results reveal that the effect of compositional change on the GFA of Cu-Zr alloys differs from $Cu_{64}Zr_{36}$ to $Cu_{50}Zr_{50}$, which has not been clarified in previous studies [11,16–18]. Moreover, the maxima in the interfacial free energy indicate that the small change of Zr concentration causes significantly different local structure in SROs and MROs of Cu-Zr liquids and crystals, resulting in higher stability of liquid and glass affecting the GFA in different ways. The present results will provide a way to improve the GFA of BMGs by adding or changing elements.

The authors thank Wonhyuk Jo, Chang-Hwan Yoo, and Yong Chan Cho for technical support of ESL, and Byeongchan Lee, Dongwoo Lee, and Kenneth F. Kelton for useful discussion and comments. This research was supported by the Converging Research Center Program through the Ministry of Science, ICT and Future Planning, Korea (Grants No. NRF-2014M3C1A8048818 and No. NRF-2014M1A7A1A01030128), and Korea Research Institute of Standards and Science (KRISS – 2017 – GP2017-0029).

[1] Z. P. Lu and C. T. Liu, J. Mater. Sci. **39**, 3965 (2004).
[2] N. Chen, L. Martin, D. V. Luzguine-Luzgin, and A. Inoue, Materials (Basel). **3**, 5320 (2010).
[3] C. T. Liu and Z. P. Lu, Intermetallics **13**, 415 (2005).
[4] W. Wang, Prog. Mater. Sci. **52**, 540 (2007).
[5] D. Turnbull, Contemp. Phys. **10**, 473 (1969).
[6] A. Inoue, Acta Mater. **48**, 279 (2000).
[7] Z. P. Lu and C. T. Liu, Acta Mater. **50**, 3501 (2002).
[8] M. Ouchetto, B. Elouadi, and S. Parke, Phys. Chem. Glass. **32**, 22 (1991).
[9] A. Takeuchi and A. Inoue, Mater. Sci. Eng. A **375–377**, 449 (2004).
[10] C. W. Ryu, D. H. Kang, S. Jeon, G. W. Lee, and E. S. Park, APL Mater. **5**, 106103 (2017).
[11] Y. Li, Q. Guo, and J. A. Kalb, Science **322**, 1816 (2008).
[12] C. Chattopadhyay and B. S. Murty, Scr. Mater. **116**, 7 (2016).
[13] A. Inoue, W. Zhang, T. Zhang, and K. Kurosaka, Acta Mater. **49**, 2645 (2001).
[14] K. W. Park, J. il Jang, M. Wakeda, Y. Shibutani, and J. C. Lee, Scr. Mater. **57**, 805 (2007).
[15] L. Yang, G. Q. Guo, L. Y. Chen, C. L. Huang, T. Ge, D. Chen, P. K. Liaw, K. Saksl, Y. Ren, Q. S. Zeng, B. LaQua, F. G. Chen, and J. Z. Jiang, Phys. Rev. Lett. **109**, 105502 (2012).
[16] J. C. Bendert, A. K. Gangopadhyay, N. A. Mauro, and K. F. Kelton, Phys. Rev. Lett. **109**, 185901 (2012).
[17] L. Xia, S. S. Fang, Q. Wang, Y. D. Dong, and C. T. Liu, Appl. Phys. Lett. **88**, 171905 (2006).
[18] C. Y. Yu, X. J. Liu, J. Lu, G. P. Zheng, and C. T. Liu, Sci. Rep. **3**, 2124 (2013).
[19] C. Tang and P. Harrowell, Nat. Mater. **12**, 507 (2013).
[20] D.-H. Kang, H. Zhang, H. Yoo, H. H. Lee, S. Lee, G. W. Lee, H. Lou, X. Wang, Q. Cao, D. Zhang, and J. Jiang, Sci. Rep. **4**, 5167 (2014).
[21] F. C. Frank, Proc. R. Soc. Lond. A. Math. Phys. Sci. **215**, 43 (1952).
[22] G. W. Lee, A. K. Gangopadhyay, T. K. Croat, T. J. Rathz, R. W. Hyers, J. R. Rogers, and K. F. Kelton, Phys. Rev. B **72**, 174107 (2005).
[23] G. W. Lee, A. K. Gangopadhyay, R. W. Hyers, T. J. Rathz, J. R. Rogers, D. S. Robinson, A. I. Goldman, and K. F. Kelton, Phys. Rev. B **77**, 184102 (2008).

[24] K. F. Kelton, G. W. Lee, A. K. Gangopadhyay, R. W. Hyers, T. J. Rathz, J. R. Rogers, M. B. Robinson, and D. S. Robinson, Phys. Rev. Lett. **90**, 195504 (2003).
[25] T. H. Kim, G. W. Lee, A. K. Gangopadhyay, R. W. Hyers, J. R. Rogers, A. I. Goldman, and K. F. Kelton, J. Phys. Condens. Matter **19**, 455212 (2007).
[26] G. W. Lee, Y. C. Cho, B. Lee, and K. F. Kelton, Phys. Rev. B **95**, 054202 (2017).
[27] P. J. Steinhardt, D. R. Nelson, and M. Ronchetti, Phys. Rev. B **28**, 784 (1983).
[28] H. Jónsson and H. C. Andersen, Phys. Rev. Lett. **60**, 2295 (1988).
[29] F. Yonezawa, Solid State Phys. **45**, 179 (1991).
[30] J. Taffs and C. Patrick Royall, Nat. Commun. **7**, 13225 (2016).
[31] K. J. Laws, D. B. Miracle, and M. Ferry, Nat. Commun. **6**, 8123 (2015).
[32] L. Ward, D. Miracle, W. Windl, O. N. Senkov, and K. Flores, Phys. Rev. B **88**, 134205 (2013).
[33] H. L. Peng, M. Z. Li, W. H. Wang, C. Wang, and K. M. Ho, Appl. Phys. Lett. **96**, 021901 (2010).
[34] N. Jakse and A. Pasturel, Phys. Rev. B **78**, 214204 (2008).
[35] M. Li, C. Z. Wang, S. G. Hao, M. J. Kramer, and K. M. Ho, Phys. Rev. B **80**, 184201 (2009).
[36] T. Abe, M. Shimono, M. Ode, and H. Onodera, Acta Mater. **54**, 909 (2006).
[37] W. Yang, F. Liu, H. Liu, H. F. Wang, Z. Chen, and G. C. Yang, J. Alloys Compd. **484**, 702 (2009).
[38] Y. Sato, C. Nakai, M. Wakeda, and S. Ogata, Sci. Rep. **7**, 7194 (2017).
[39] See Supplemental Material at http://link.aps.org/supplemental/10.1103/PhysRevMaterials.2.115606 for experimental details of underccoling, density, viscosity, DSC, TTT curves, estimation of interfacial energy, and a list of thermophysical parameters obtained from the measurements.
[40] C. J. Smithells, *Smithells Metals Reference Book*, 8th ed. (Elsevier Butterworth-Heinemann, New York, 2004).
[41] H. Okamoto, J. Phase Equilib. Diffus. **29**, 204 (2008).
[42] K. F. Kelton, Solid State Phys. **45**, 75 (1991).
[43] L. Ge, X. Hui, E. R. Wang, G. L. Chen, R. Arroyave, and Z. K. Liu, Intermetallics **16**, 27 (2008).
[44] F. Gillessen and D. M. Herlach, Mater. Sci. Eng. **97**, 147 (1988).
[45] M. B. Tang, D. Q. Zhao, M. X. Pan, and W. H. Wang, Chinese Phys. Lett. **21**, 901 (2004).
[46] D. Wang, S. J. Zhao, and L. M. Liu, J. Phys. Chem. A **119**, 806 (2015).
[47] F. Spaepen and R. B. Meyer, Scr. Metall. **10**, 37 (1976).
[48] S. Mukherjee, J. Schroers, W. L. Johnson, and W.-K. K. Rhim, Phys. Rev. Lett. **94**, 245501 (2005).
[49] W. L. Johnson, J. H. Na, and M. D. Demetriou, Nat. Commun. **7**, 10313 (2016).